

Perturbation efficiency resolves target-count bias in network proximity metrics: A controlled audit

Antony Bevan^{1,*}

¹Department of Pharmacognosy, Madurai Medical College, Madurai, India

*Corresponding author: antonybevan04@gmail.com

4 Abstract

5 Network-based metrics are widely used to identify associations between compounds and diseases, as
6 suming that proximity within a protein–protein interaction network reflects functional relevance. How-
7 ever, these metrics are often reported as Z-scores, which we demonstrate are fundamentally sensitive to
8 the number of targets a compound possesses. This dependency introduces a systematic bias where com-
9 pounds with broad polypharmacology appear statistically significant due to null distribution tightening
10 (the Law of Large Numbers) rather than physical network reachability. Here, we systematically audit
11 this bias using the human liver interactome and a controlled comparison of two constituents from *Hy-*
12 *pericum perforatum*. We show that conventional proximity Z-scores yield unstable rankings that reverse
13 depending on network construction parameters. While a compound with many targets may achieve a
14 higher Z-score, it can remain physically more distant from the disease module than a compound with
15 fewer, high-leverage targets. We resolve this by utilizing random walk–based influence propagation and
16 applying a size-normalized metric, perturbation efficiency, to ensure unbiased comparisons. Our results
17 show that influence-based rankings are stable across varied network thresholds and correctly identify
18 high-leverage modulators that proximity metrics miss. This study provides a methodological template
19 for identifying and correcting statistical artifacts in network medicine, enabling more reliable risk assess-
20 ment in complex biological systems.

Keywords: network medicine, proximity metrics, metric robustness, drug-induced liver injury, polypharmacology, Z-score bias, Law of Large Numbers, perturbation efficiency.

23 1 Introduction

24 Network-based prioritization is a cornerstone of modern systems biology and drug discovery, assuming
25 that the topological proximity between compound targets and disease genes within a protein–protein in-
26 teraction (PPI) network reflects functional relevance [1–4]. Because raw network distances are sensitive
27 to local topology and degree distribution, they are typically reported as Z-scores relative to degree-
28 matched null models. While these Z-scores successfully quantify statistical significance in most applica-
29 tions [3], we demonstrate they can be confounded by large asymmetries in target set size. As the number
30 of seed nodes increases, the variance of the null distribution decreases (the Law of Large Numbers),
31 leading to deterministic significance inflation for compounds with broad polypharmacology. Identifying
32 whether such results reflect true biological influence, or whether they represent systematic artifacts of
33 distance-based inference, is essential for the reliability of network medicine.

34 Using the human liver interactome as a model system, we investigate this confounding effect through
35 a controlled comparison of two constituents from *Hypericum perforatum* (St. John’s Wort). These con-
36 stituents—Hyperforin and Quercetin—exhibit highly asymmetric target set sizes: Hyperforin possesses
37 10 validated targets, while Quercetin has over 60 [5–7]. This system serves as a controlled model because
38 it pairs a known biological ground truth (Hyperforin-mediated PXR activation) with extreme topolog-
39 ical asymmetry, providing a sharp stress test for network metrics. Conventional proximity Z-scores
40 predict greater disease-associated significance for the broad-spectrum modulator, even when it is phys-
41 ically more distant from the disease module than the high-leverage modulator. This reversal indicates
42 that proximity-based prioritization is unstable across network construction parameters and susceptible to
43 sample-size artifacts.

44 Here, we evaluate the robustness of proximity-based and influence-based metrics for comparative pri-
45 oritization. We demonstrate that proximity Z-scores yield unstable, threshold-dependent rankings driven
46 by null-distribution tightening rather than physical reachability. To resolve this instability, we utilize ran-
47 dom walk–based influence propagation, which integrates over the entire network topology and captures
48 signal amplification through regulatory hubs [8]. We apply a normalized metric, perturbation efficiency,
49 to account for target set size and ensure unbiased comparisons. Our results show that influence-based
50 propagation provides a stable, theoretically consistent framework for network pharmacology that cor-
51 rectly identifies high-leverage perturbations where traditional proximity metrics fail.

52 **2 Results**

53 **2.1 Proximity Z-scores are confounded by target set size**

54 We first established network context by quantifying target count and shortest-path proximity to 82 DILI-
55 associated genes (Figure 1). Quercetin engages 62 targets in the liver-expressed largest connected
56 component; Hyperforin engages 10. At STRING confidence ≥ 900 , Hyperforin targets are physically
57 closer to DILI genes ($d_c = 1.30$) than Quercetin targets ($d_c = 1.68$; Table 1). However, the proxim-
58 ity Z-scores yield the opposite ranking: Quercetin achieves $Z = -5.44$ ($p < 0.001$), while Hyperforin
59 achieves $Z = -3.86$ ($p < 0.001$). All reported associations survived Benjamini–Hochberg FDR correc-
60 tion ($q < 0.05$).

61 This statistical artifact suggests that Quercetin poses greater risk, whereas the physical topology fa-
62 vors Hyperforin. This effect occurs independently of network construction parameters and represents a
63 fundamental statistical property of averaged distributions: larger samples inherently produce more pre-
64 cise (narrower) null distributions, artificially inflating Z-score magnitude regardless of actual topological
65 proximity. This is a manifestation of the Law of Large Numbers (LLN).

66 **2.2 Influence-based rankings are stable and resolve the confound**

67 Random walk with restart (RWR) stabilizes this ranking by integrating over all paths (Figure 2). Hyper-
68 forin achieves influence $Z = +10.12$ ($p < 0.001$); Quercetin achieves $Z = +4.55$ ($p < 0.001$; Table 1).
69 Unlike proximity, influence Z-scores correctly reflect the topological advantage of Hyperforin’s regu-
70 latory hub occupancy. This ranking aligns with the known biological ground truth: Hyperforin is the
71 hepatotoxic constituent responsible for drug-drug interactions via PXR activation, while Quercetin has
72 no documented hepatotoxicity and may be hepatoprotective. The ranking remains consistent across
73 topology-only and expression-weighted analyses, demonstrating that influence propagation is less sus-
74 ceptible to sample-size artifacts than shortest-path distance.

75 **2.3 Expression weighting refines the signal**

76 To assess whether the RWR signal persists under tissue-specific constraint, we applied expression-
77 weighted influence propagation (EWI), weighting transitions by destination-node liver expression (Fig-
78 ure 3).

79 The Z-score differential narrows but remains substantial under expression weighting: Hyperforin
80 $Z = +8.98$ ($p < 0.001$); Quercetin $Z = +5.79$ ($p < 0.001$). Hyperforin’s advantage is driven primarily

81 by the PXR–CYP master regulatory axis, which remains highly active in liver tissue (e.g., CYP3A4 at
82 335 TPM). Quercetin’s influence is moderated by its broad, diffuse target profile, which includes several
83 high-expression nodes (e.g., CFB at 1,115 TPM) that do not converge on a DILI effector hub.

84 **2.4 Normalizing for target count confirms Hyperforin’s topological advantage**

85 To resolve the target-count paradox, we compared the average network influence of each individual
86 target, reframing polypharmacology as an efficiency problem rather than a coverage problem (Figure 4;
87 Table 2).

| Compound | Targets | Eff. (RWR) | Eff. (EWI) | RWR Ratio* | EWI Ratio† |
|------------------------|---------|------------|------------|--------------------|--------------------|
| Hyperforin | 10 | 0.1138 | 0.1330 | — | — |
| Quercetin | 62 | 0.0322 | 0.0493 | — | — |
| Fold difference | — | — | — | 3.5× (3.7×) | 2.7× (2.8×) |

89 *RWR Ratio: observed ratio (robust ratio in parentheses). †EWI Ratio: observed ratio (robust ratio in paren-
90 theses).

91 Each Hyperforin target contributes 3.7× more DILI-directed influence than each Quercetin target (robust ra-
92 tio). This disparity indicates that Hyperforin’s target positions are substantially higher leverage than those of
93 Quercetin, achieving greater perturbation efficiency despite a 6-fold smaller target set. The efficiency ratio re-
94 mains stable within a narrow range: 3.7× at STRING ≥ 700 , 3.5× at ≥ 900 (a 5% variation despite 33% reduction
95 in network density). In contrast, proximity Z-score rankings undergo complete reversal between these thresholds.
96 This demonstrates that perturbation efficiency is a parameter-invariant comparative metric where distance-based
97 Z-scores are not.

98 **2.5 Bootstrap resampling excludes target-selection bias**

99 To rule out the possibility that Hyperforin’s advantage arises from favorable target selection rather than strategic
100 network positioning, we performed bootstrap sensitivity analysis (Figure 5). 100 random 10-target subsets were
101 sampled without replacement from Quercetin’s 62-target pool and scored by RWR.

102 Hyperforin’s observed influence (0.1138) exceeds the entire bootstrap distribution from Quercetin (mean =
103 0.0308, 95% CI = [0.0160, 0.0542]; Table 3). The fold difference between Hyperforin and the bootstrap mean is
104 3.7×. This confirms that Hyperforin’s advantage is not an artifact of target count; even when sampling equalized
105 subsets from Quercetin’s pool, no configuration matches Hyperforin’s influence.

106 **2.6 Ranking stability across network thresholds**

107 The influence ranking is stable across network confidence thresholds (Table 6). Hyperforin ranks first in all RWR
108 and EWI configurations at both ≥ 700 and ≥ 900 thresholds. Notably, the proximity ranking reverses between
109 thresholds: at ≥ 700 , Hyperforin is physically closer ($d_c = 0.60$ vs 1.34) and more "significant" ($Z = -6.04$ vs
110 -5.46). At ≥ 900 , Quercetin appears more "significant" ($Z = -5.44$ vs -3.86) despite being physically more dis-
111 tant (1.68 vs 1.30). This instability in proximity Z-scores—while influence rankings remain stable—demonstrates
112 that influence-based metrics are more robust to network construction parameters.

113 **2.7 Chemical similarity excludes structural confounding**

114 To exclude the possibility that Hyperforin's network signal reflects structural similarity to known hepatotoxins,
115 we performed chemical similarity analysis against the DILrank reference set (Figure 6). Morgan fingerprints
116 (ECFP4) revealed that neither compound exceeds the 0.4 Tanimoto threshold for structural analog detection. No-
117 tably, Quercetin exhibits higher structural similarity to DILI reference drugs yet lower network influence, reinforc-
118 ing that the observed asymmetry is driven by network topology rather than chemical features.

119 **3 Discussion**

120 **3.1 Ranking stability and the Z-score confound**

121 The results of this study highlight a potential limitation in the use of network proximity Z-scores when comparing
122 compounds with asymmetric target set sizes. While proximity is a standard prioritization criterion, our analysis
123 demonstrates that its significance rankings can be influenced by the target count rather than topological distance
124 alone. As the number of targets increases, the variance of the null distribution decreases (a manifestation of the Law
125 of Large Numbers), which can lead to inflated significance levels for compounds with broad polypharmacology. In
126 our controlled comparison, this effect causes a reversal of proximity-based rankings between network thresholds,
127 failing to accurately reflect the physical distance advantage of a high-leverage modulator.

128 Influence-based metrics (RWR and EWI) appear less sensitive to this particular artifact. By integrating over the
129 entire network topology, these methods capture signal propagation through regulatory hubs, providing rankings that
130 remain stable across different network construction parameters. This relative stability suggests that influence-based
131 propagation may offer a more robust framework for comparative network medicine, particularly in the presence of
132 incomplete or asymmetric pharmacological data.

133 The mechanistic explanation for this robustness is that RWR integrates over *all* paths, capturing how signals
134 amplify through hubs like PXR and AKT1. Shortest-path proximity, by contrast, is a descriptive metric for min-
135 imum reachability; treating it as an inferential surrogate for functional impact conflates topological context with
136 biological consequence.

137 **3.2 Relationship to prior work**

138 Our findings do not contradict the foundational work of Guney et al. (2016), but rather identify a specific failure
139 mode that their study design did not stress-test. Guney et al. evaluated network proximity as a classifier for drug-
140 disease associations across 238 drugs with a mean of 3.5 targets per drug—a relatively homogeneous dataset.
141 They reported that proximity is “not biased with respect to the number of targets a drug has” and found that the
142 closest-distance measure (d_c) outperformed a diffusion kernel measure (d_k) for binary classification [3].

143 Our study addresses a fundamentally different question: *comparative ranking* of two compounds with highly
144 asymmetric target counts (10 vs. 62). In this regime, the variance-shrinkage artifact becomes a first-order problem.
145 Guney’s kernel benchmark (d_k) is related to but distinct from random walk with restart; d_k sums contributions from
146 all weighted paths, whereas RWR iteratively propagates probability mass with a restart factor that anchors the walk
147 to seed nodes. More critically, neither d_c nor d_k provides a principled normalization for target set size.

148 A primary methodological resolution proposed in this study is the use of *perturbation efficiency*: the average
149 influence exerted per target. This normalization resolves the target-count paradox regardless of whether the under-
150 lying propagation method is shortest-path, kernel, or random walk. By framing polypharmacology as an efficiency
151 problem rather than a coverage problem, we provide a bias-corrected comparative framework that survives ro-
152 bustness checks where raw Z-scores fail. While Guney et al. found that a diffusion kernel underperformed closest
153 distance for binary classification of known drug-disease pairs, our task differs fundamentally: we address compara-
154 tive ranking under extreme target-count asymmetry (10 vs. 62 targets). RWR’s restart mechanism enforces locality
155 absent in pure diffusion kernels, and our empirical results demonstrate stable rankings that align with biological
156 ground truth—a criterion not assessed in Guney’s benchmark.

157 **3.3 Expression weighting as a biological constraint**

158 Expression-weighted influence (EWI) constrains signal propagation to liver-active nodes. By attracting signal to
159 highly expressed proteins (destination-node weighting), we ensure that the network propagation reflects tissue-
160 specific biology. Under this constraint, the Hyperforin advantage persists, demonstrating that its topological ef-
161 ficiency is not an artifact of an unconstrained PPI network but is supported by the expression profile of the liver.
162 Attenuation of signal is expected when walks are constrained to active pathways; the fact that the ranking remains
163 stable provides positive evidence for the biological relevance of the PXR axis.

164 **3.4 Perturbation efficiency vs. topological coverage**

165 By normalizing total influence for target set size (where the restart vector is already $|T|$ -weighted), we provide
166 a more balanced comparison of perturbation efficiency. Our results show that a single Hyperforin target exerts
167 3.7-fold more influence on the DILI module than a Quercetin target.

168 This efficiency claim is further validated by bootstrap sensitivity analysis. Even when sampling size-matched
169 10-target subsets from Quercetin’s pool, none reached the influence level achieved by Hyperforin. This demon-

170 strates that the advantage is not due to target count, but to the strategic network position of Hyperforin's tar-
171 gets—specifically their convergence on the PXR master regulator and downstream CYP effectors.

172 **3.5 Mechanistic context: The PXR axis**

173 The stability of the influence ranking aligns with the well-characterized PXR–CYP master regulatory axis. Hyper-
174 forin's primary target, NR1I2 (PXR), induces the expression of major xenobiotic metabolism enzymes including
175 CYP3A4 and CYP2C9 [6, 9]. In our network analysis, these effectors are part of the target set and the DILI
176 module, creating a high-connectivity hub structure that enables efficient propagation. Quercetin's 62 targets, while
177 numerous, are distributed across redundant or peripheral pathways that do not converge on a regulatory bottleneck.
178 Furthermore, clinical evidence indicates that Quercetin is not associated with hepatotoxicity and may exhibit hep-
179 atoprotective properties [7, 10]. Recent experimental studies have corroborated that St. John's wort exacerbates
180 hepatotoxicity through precisely this PXR-mediated bioactivation mechanism [11].

181 **3.6 Limitations**

182 Several limitations warrant consideration. First, network influence is a measure of topological reach and pertur-
183 bation potential, not a direct surrogate for toxicological outcomes. This model is dose-independent and does not
184 account for pharmacokinetics, binding affinity, or saturation kinetics. A high influence score indicates that a com-
185 pound's targets are strategically positioned to modulate a disease module, but the actual biological effect depends
186 on the molecular mechanism of action (e.g., agonism vs. antagonism) and the kinetic context.

187 Second, while we demonstrate that proximity Z-scores are confounded by target set size, influence-based Z-
188 scores are not entirely immune to this effect. As the number of seed nodes increases, the variance of the null
189 distribution for influence sums also decreases, though less severely than for distance-based metrics. Critically,
190 our core claims do not rest on absolute Z-score comparisons. We demonstrate that influence-based *rankings* are
191 stable across network thresholds, while proximity rankings are not. We further resolve the size-dependence by
192 introducing perturbation efficiency (influence per target), which explicitly normalizes for target count and provides
193 a bias-corrected comparative metric.

194 Third, our case study is limited to a single botanical with two contrasting constituents. While this provides a
195 controlled minimal model, generalization to larger compound libraries will require further validation.

196 **3.7 Conclusions**

197 In this study, we utilized *H. perforatum* as a known toxicological model to validate the *reliability* of network
198 metrics; the biological ground truth (Hyperforin-mediated PXR activation) allowed us to confirm that influence
199 propagation correctly identifies high-leverage perturbations where proximity metrics fail. The methodological
200 conclusion is that proximity Z-scores are susceptible to sample-size confounding and should be used descriptively
201 rather than for comparative inference across compounds with differing target counts. Influence-based propagation,

202 combined with per-target normalization, provides a more stable framework that survives robustness checks and
203 aligns better with mechanistic reality.

204 More broadly, this work provides a methodological template for identifying and resolving metric artifacts
205 in network toxicology. By integrating signed edge weights and transcriptometric data, future iterations of this
206 framework could investigate phenotype-specific associations, linking topological influence on specific biological
207 sub-modules to discrete clinical outcomes.

208 4 Methods

209 4.1 Data sources

210 4.1.1 Protein–protein interaction network

211 Human protein–protein interactions were obtained from STRING v12.0 [12]. Combined confidence scores were
212 computed per STRING methodology (text mining, experiments, databases, co-expression, neighborhood, gene
213 fusion, co-occurrence). Only edges with combined confidence ≥ 900 (highest confidence tier) were retained. Raw
214 network: 11,693 genes, 100,383 edges.

215 4.1.2 Liver expression data

216 Gene expression data were obtained from the Genotype-Tissue Expression Project (GTEx) v8 [13]. Median tran-
217 scripts per million (TPM) values for liver tissue were extracted from the 2017-06-05 release (RNASeQCv1.1.9).
218 Genes with liver TPM ≥ 1 were retained. Result: 13,496 liver-expressed genes.

219 4.1.3 Drug-induced liver injury gene set

220 DILI-associated genes were obtained from DisGeNET [14] curated gene-disease associations. Query: UMLS
221 concept identifier C0860207 (Drug-Induced Liver Injury). Inclusion criterion: genes with curated evidence linking
222 to DILI. Raw DILI gene count: 127 genes.

223 4.1.4 Hyperforin targets

224 Hyperforin targets were curated from primary literature sources [6, 9]. Sources included studies of PXR activation,
225 CYP induction, and ABC transporter modulation. Raw target count: 14 proteins (Table 5).

226 4.1.5 Quercetin targets

227 Quercetin targets were retrieved programmatically from ChEMBL v31 [15] via REST API. Query: CHEMBL159
228 (Quercetin). Filter: human targets with experimentally validated bioactivity (IC_{50} , K_i , or $EC_{50} \leq 10 \mu M$). Raw
229 target count: 122 proteins.

230 **4.2 Target processing**

231 Protein identifiers were mapped to HUGO gene symbols using STRING info files and UniProt [16]. Non-human
232 proteins (mouse, rat, bacterial, viral) were excluded. Gene symbols were standardized (e.g., MDR1 → ABCB1).
233 Processed target counts: Hyperforin = 14, Quercetin = 87.

234 **4.3 Network construction**

235 The STRING network was filtered to genes with liver expression ≥ 1 TPM (GTEx v8). The largest connected
236 component (LCC) was extracted using NetworkX [17]. Compound targets and DILI genes not present in the LCC
237 were excluded. Final network: 7,677 nodes, 66,908 edges. Final target counts: Hyperforin = 10, Quercetin = 62.
238 Final DILI gene count: 82.

239 Five genes are targeted by both compounds: ABCG2, AKT1, CYP3A4, MMP2, MMP9. These were retained
240 in both target sets.

241 **4.4 Shortest-path proximity (descriptive)**

242 Mean minimum shortest-path distance from compound targets T to DILI genes D :

$$d_c = \frac{1}{|T|} \sum_{t \in T} \min_{d \in D} \text{dist}(t, d) \quad (1)$$

243 where $\text{dist}(t, d)$ is the unweighted shortest-path length in the LCC. Shortest-path proximity is a descriptive metric.
244 It was used to provide network context, not to test influence.

245 **4.5 Random walk with restart**

246 Influence propagation was quantified using random walk with restart (RWR), a global network propagation al-
247 gorithm that captures both direct and indirect associations by simulating the diffusion of signal from seed nodes
248 [3, 8]. Given an adjacency matrix \mathbf{A} , we define the column-normalized transition matrix \mathbf{W} as:

$$W_{ij} = \frac{A_{ij}}{\sum_k A_{kj}} \quad (2)$$

249 The steady-state probability vector \mathbf{p} is solved iteratively until convergence:

$$\mathbf{p}^{(k+1)} = (1 - \alpha)\mathbf{W}\mathbf{p}^{(k)} + \alpha\mathbf{p}_0 \quad (3)$$

250 where:

- 251 • $\alpha = 0.15$ is the restart probability (teleportation factor), ensuring the walk remains local to the seeds.
252 • \mathbf{p}_0 is the restart (seed) vector, with $p_0(i) = 1/|T|$ for $i \in T$ (targets) and 0 otherwise.

- 253 • Convergence is defined as the L_1 norm of the difference between successive iterations being $< 10^{-6}$.
- 254 All computations reached convergence within 100 iterations. The total influence I on the DILI module D is the
 255 sum of steady-state probabilities at disease nodes: $I = \sum_{d \in D} p(d)$.

256 **4.6 Permutation testing and degree matching**

257 To assess whether the observed influence I is significantly greater than what would be expected by chance, we
 258 performed permutation testing ($n = 1,000$). To account for the bias where high-degree nodes (hubs) naturally
 259 accumulate more influence, we utilized a degree-preserving sampling strategy. For each target $t \in T$, a random
 260 surrogate node was sampled from the network such that its degree k_{rand} was within $\pm 25\%$ of the original target's
 261 degree k_t . This ensures that the null distribution reflects the connectivity profile of the original target set. Random
 262 seeds were fixed to 42 for reproducibility. Z-scores were computed as $Z = (x_{obs} - \mu_{null})/\sigma_{null}$, and empirical
 263 P -values were derived from the null distribution.

264 **4.7 Expression-weighted influence**

265 Edge weights were modified by destination-node liver expression:

$$W'_{ij} = \frac{A_{ij} \cdot e_i}{\sum_k A_{kj} \cdot e_k} \quad (4)$$

266 where e_i is the normalized liver expression for gene i (GTEx v8 liver). Liver TPM values were log-transformed
 267 ($\log_2(\text{TPM} + 1)$) and min-max normalized to [0, 1] across the network. A minimum expression floor of 0.01 was
 268 applied to ensure all nodes remained reachable. Attracting signal to highly-expressed nodes constrains RWR
 269 propagation to biologically active pathways in the liver. All other RWR parameters were identical. Random seed:
 270 42.

271 **4.8 Quantifying perturbation efficiency**

272 By defining the restart vector as $\mathbf{p}_0(i) = 1/|T|$ (Eq. 75), the total steady-state probability mass \mathbf{p} is inherently
 273 partitioned among the target set. Consequently, the summed influence I on the DILI module (Eq. 81) represents
 274 the average perturbation efficiency per target. This normalization serves as an effect-size adjustment that allows
 275 for a direct comparison of the per-unit impact of compounds with asymmetric target sets. Hereafter, we refer to
 276 this as the perturbation efficiency.

277 **4.9 Bootstrap sensitivity analysis**

278 To assess whether target count explains the observed ranking: 100 random 10-target subsets were sampled without
 279 replacement from Quercetin's 62-target pool. Each subset was scored by standard RWR. Summary statistics: mean,

280 standard deviation, 95th percentile. The observed Hyperforin influence was compared to the bootstrap distribution.
281 Random seed: 42.

282 **4.10 Chemical similarity analysis**

283 Structural similarity to known hepatotoxins was assessed to exclude confounding by chemical class. Morgan
284 fingerprints (ECFP4; radius = 2, 2048 bits) were generated using RDKit v2023.03 [18]. Reference set: DILIrank
285 2.0 drugs with retrievable SMILES (542 DILI-positive, 365 DILI-negative). SMILES were retrieved via PubChem
286 REST API. Tanimoto coefficient:

$$\text{Tanimoto}(A, B) = \frac{|A \cap B|}{|A \cup B|} \quad (5)$$

287 Maximum similarity across the reference set was reported for each compound. Structural analog threshold: Tani-
288 moto > 0.4 [19].

289 **4.11 Software and reproducibility**

290 Python 3.10, NetworkX 3.1 [17]; R 4.3, igraph 1.5. All random seeds fixed at 42. Target lists sorted alphabetically
291 before processing.

292 **4.12 Code and data availability**

293 All code: <https://github.com/antonybevan/h-perforatum-network-tox>

294 Data sources:

- 295 • STRING v12.0: <https://string-db.org>
296 • GTEx v8: <https://gtexportal.org>
297 • ChEMBL v31: <https://www.ebi.ac.uk/chembl>
298 • DILIRank 2.0: <https://www.fda.gov/science-research/ltrkb>

299 **References**

- 300 [1] Andrew L Hopkins. Network pharmacology: the next paradigm in drug discovery. *Nature Chemical Biology*,
301 4(11):682–690, 2008. doi: 10.1038/nchembio.118.
- 302 [2] Albert-László Barabási, Natali Gulbahce, and Joseph Loscalzo. Network medicine: a network-based ap-
303 proach to human disease. *Nature Reviews Genetics*, 12(1):56–68, 2011. doi: 10.1038/nrg2918.
- 304 [3] Emre Guney, Jörg Menche, Marc Vidal, and Albert-László Barabási. Network-based in silico drug efficacy
305 screening. *Nature Communications*, 7:10331, 2016. doi: 10.1038/ncomms10331.

- 306 [4] Jörg Menche, Amitabh Sharma, Maksim Kitsak, Susan Dina Ghiassian, Marc Vidal, Joseph Loscalzo, and
307 Albert-László Barabási. Uncovering disease-disease relationships through the incomplete interactome. *Science*, 347(6224):1257601, 2015. doi: 10.1126/science.1257601.
- 309 [5] Adolf Nahrstedt and Veronika Butterweck. Biologically active and other chemical constituents of the herb of
310 Hypericum perforatum L. *Pharmacopsychiatry*, 30(S2):129–134, 1997. doi: 10.1055/s-2007-979533.
- 311 [6] Linda B Moore, Bryan Goodwin, Stacey A Jones, G Bruce Wisely, Connie J Serabjit-Singh, Timothy M
312 Willson, John L Collins, and Steven A Kliewer. St. John's wort induces hepatic drug metabolism through
313 activation of the Pregnen X Receptor. *Proceedings of the National Academy of Sciences*, 97(13):7500–7502,
314 2000. doi: 10.1073/pnas.130155097.
- 315 [7] Agnes W Boots, Guido RMM Haenen, and Aalt Bast. Health effects of quercetin: from antioxidant to
316 nutraceutical. *European Journal of Pharmacology*, 585(2-3):325–337, 2008. doi: 10.1016/j.ejphar.2008.03
317 .008.
- 318 [8] Sebastian Köhler, Sebastian Bauer, Denise Horn, and Peter N Robinson. Walking the interactome for prior-
319 itization of candidate disease genes. *The American Journal of Human Genetics*, 82(4):949–958, 2008. doi:
320 10.1016/j.ajhg.2008.02.013.
- 321 [9] Reginald E Watkins, G Bruce Wisely, Linda B Moore, John L Collins, Millard H Lambert, Shawn P Williams,
322 Timothy M Willson, Steven A Kliewer, and Matthew R Redinbo. The human nuclear xenobiotic receptor
323 PXR: structural determinants of directed promiscuity. *Science*, 292(5525):2329–2333, 2001. doi: 10.1126/
324 science.1060762.
- 325 [10] National Institute of Diabetes and Digestive and Kidney Diseases. LiverTox: Clinical and research informa-
326 tion on drug-induced liver injury [internet]. quercetin. <https://www.ncbi.nlm.nih.gov/books/NBK548281/>, 2020. Updated July 10, 2020.
- 328 [11] Siyu Chen, Xue Wang, Xinran Ye, Qinjin Wang, Xin Sun, Chunyan Ma, Zhidong Yuan, and Yang Yu. St.
329 John's wort exacerbates acetaminophen-induced liver injury through PXR and CYP-mediated bioactivation.
330 *Toxicological Sciences*, 190(1):68–80, 2022. doi: 10.1093/toxsci/kfac098.
- 331 [12] Damian Szklarczyk, Rebecca Kirsch, Mikaela Koutrouli, Katerina Nastou, Farrokh Mehryary, Radja
332 Hachilif, Annika L Gable, Tao Fang, Nadezhda T Doncheva, Sampo Pyysalo, Peer Bork, Lars J Jensen, and
333 Christian von Mering. The STRING database in 2023: protein–protein association networks and functional
334 enrichment analyses for any sequenced genome of interest. *Nucleic Acids Research*, 51(D1):D483–D489,
335 2023. doi: 10.1093/nar/gkac1000.
- 336 [13] GTEx Consortium. The GTEx Consortium atlas of genetic regulatory effects across human tissues. *Science*,
337 369(6509):1318–1330, 2020. doi: 10.1126/science.aaz1776.

- 338 [14] Janet Piñero, Juan Manuel Ramírez-Anguita, Josep Saüch-Pitarch, Francesco Ronzano, Emilio Centeno,
339 Ferran Sanz, and Laura I Furlong. The DisGeNET knowledge platform for disease genomics: 2019 update.
340 *Nucleic Acids Research*, 48(D1):D845–D855, 2020. doi: 10.1093/nar/gkz1021.
- 341 [15] David Mendez, Anna Gaulton, A Patrícia Bento, Jon Chambers, Marleen De Veij, Eloy Félix, María Paula
342 Magaña, Juan F Mosquera, Prudence Mutowo, Michał Nowotka, Maria Gordillo-Marañón, Fiona Hunter,
343 Laura Junco, Grace Mugumbate, Milagros Rodriguez-Lopez, Francis Atkinson, Nicolas Bosc, Chris J
344 Radoux, Aldo Segura-Cabrera, Anne Hersey, and Andrew R Leach. ChEMBL: towards direct deposition
345 of bioassay data. *Nucleic Acids Research*, 47(D1):D930–D940, 2019. doi: 10.1093/nar/gky1075.
- 346 [16] UniProt Consortium. UniProt: the Universal Protein Knowledgebase in 2023. *Nucleic Acids Research*, 51
347 (D1):D483–D489, 2023. doi: 10.1093/nar/gkac1052.
- 348 [17] Aric A Hagberg, Daniel A Schult, and Pieter J Swart. Exploring network structure, dynamics, and function
349 using NetworkX. In Gaël Varoquaux, Travis Vaught, and Jarrod Millman, editors, *Proceedings of the 7th*
350 *Python in Science Conference (SciPy 2008)*, pages 11–15, 2008.
- 351 [18] RDKit. RDKit: Open-source cheminformatics. <https://www.rdkit.org>, 2023. Version 2023.03.
- 352 [19] Gerald Maggiora, Martin Vogt, Dagmar Stumpfe, and Jürgen Bajorath. Molecular similarity in medicinal
353 chemistry. *Journal of Medicinal Chemistry*, 57(8):3186–3204, 2014. doi: 10.1021/jm401411z.
- 354 [20] R Scott Obach. Inhibition of human cytochrome P450 enzymes by constituents of St. John’s Wort, an herbal
355 preparation used in the treatment of depression. *Journal of Pharmacology and Experimental Therapeutics*,
356 294(1):88–95, 2000. doi: 10.1124/jpet.294.1.88.
- 357 [21] Bernard J Komoroski, Shuyan Zhang, Steven A Wrighton, Stephen C Strom, Raman Venkataraman, and
358 Erin G Schuetz. Induction and inhibition of cytochromes P450 by the St. John’s wort constituent hyperforin
359 in human hepatocytes. *Drug Metabolism and Disposition*, 32(5):512–518, 2004. doi: 10.1124/dmd.32.5.512.
- 360 [22] M Hennessy, D Kelleher, JP Lloyd, A Alrajhi, O Meenaghan, C McDonald, F Mulcahy, JP Spiers, and
361 J Feely. St John’s wort increases expression of P-glycoprotein: implications for drug interactions. *British*
362 *Journal of Clinical Pharmacology*, 53(1):75–82, 2002. doi: 10.1046/j.1365-2125.2002.01512.x.
- 363 [23] H Assefa and V Butterweck. The role of hyperforin in the metabolic and transport-mediated drug interactions
364 of St. John’s wort. *Planta Medica*, 70(4):291–300, 2004. doi: 10.1055/s-2004-818938.
- 365 [24] Er-Jia Wang, Mary Barecki-Roach, and William W Johnson. Quantitative characterization of direct P-
366 glycoprotein inhibition by St John’s wort constituents hypericin and hyperforin. *Journal of Pharmacy and*
367 *Pharmacology*, 56(11):1451–1456, 2004. doi: 10.1211/0022357044736.

- 368 [25] C Quiney, C Billard, A M Faussat, C Salanoubat, and J P Kolb. Hyperforin directly inhibits AKT1 kinase
369 activity and promotes apoptosis in AML cells. *Leukemia*, 21(10):2101–2111, 2007. doi: 10.1038/sj.leu.240
370 4834.
- 371 [26] C Quiney, C Billard, C Salanoubat, J D Fourneron, and J P Kolb. Hyperforin inhibits MMP-9 secretion by
372 B-cell chronic lymphocytic leukemia cells. *Leukemia*, 20(8):1514–1521, 2006. doi: 10.1038/sj.leu.2404283.
- 373 [27] Kristian Leuner, Viacheslav Kazanski, Marina Müller, Kirill Essin, Britta Henke, Martina Gassen, Christo-
374 pher Koch, Christina Bulut, Karola Silbermann, Annette Kopp-Schneider, Gerald Thiel, Vladimir Laketa,
375 Inna Gorshkova, Valentina Przetheskikh, Christian Harteneck, Wolfgang F Graier, Vadym Degtyar, Peter
376 Lipp, Axel Lückhoff, and Walter E Müller. Hyperforin—a key constituent of St. John’s wort specifically
377 activates TRPC6 channels. *The FASEB Journal*, 21(14):4101–4111, 2007. doi: 10.1096/fj.07-8110com.
- 378 [28] Katarina Hostanska, J Reiher, S Jessenmeyer, J Reichling, and R Saller. Hyperforin and hypericin: synergistic
379 cytotoxicity and induced apoptosis in human malignant cell lines. *European Journal of Pharmaceutics and*
380 *Biopharmaceutics*, 55(3):301–310, 2003. doi: 10.1016/s0939-6411(03)00021-3.
- 381 [29] Vikas Kumar, Alexander Mdzinarishvili, Thomas Kiewert, Maria P Abbracchio, Annalisa Pinna, Renata
382 Ciccarelli, Walter E Müller, and Jochen Klein. NMDA receptor-antagonistic properties of hyperforin, a
383 constituent of St. John’s wort. *Journal of Pharmacological Sciences*, 102(1):47–54, 2006. doi: 10.1254/jphs
384 .fp06041.

385 **Declarations**

386 **Author Contributions (CRediT)**

387 **Antony Bevan:** Conceptualization, Methodology, Software, Validation, Formal analysis, Investigation, Data Cu-
388 ration, Writing - Original Draft, Writing - Review & Editing, Visualization.

389 **Use of AI Tools**

390 AI-assisted tools were used to assist with code development and statistical analysis. The author takes full respon-
391 sibility for all content.

392 **Competing Interests**

393 The author declares no competing interests.

394 **Data Availability**

395 All data and code supporting this study are publicly available at: <https://github.com/antonybevan/h-per>
396 foratum-network-tox

397 Source data for all figures and tables are provided in the Supplementary Information. Raw data were obtained
398 from the following public repositories:

- 399 • STRING v12.0: <https://string-db.org>
- 400 • GTEx v8: <https://gtexportal.org>
- 401 • ChEMBL v31: <https://www.ebi.ac.uk/chembl>
- 402 • DisGeNET: <https://www.disgenet.org>
- 403 • DILIrank 2.0: <https://www.fda.gov/science-research/ltrkb>

404 **Code Availability**

405 All analysis code is available at: <https://github.com/antonybevan/h-perforatum-network-tox>

406 The repository includes:

- 407 • Python scripts for network construction, RWR, permutation testing
- 408 • R scripts for visualization
- 409 • Complete pipeline documentation
- 410 • Fixed random seeds for full reproducibility

411 Software versions: Python 3.10, NetworkX 3.1, NumPy 1.26, Pandas 2.1, RDKit 2023.03, R 4.3, ggplot2 3.5.

⁴¹² **Funding**

⁴¹³ This research received no external funding.

414 **Figure Legends**

415 **Figure 1. Network context: target count and physical proximity to DILI genes.** (A) Target count in the
416 liver-expressed largest connected component. Quercetin: 62 targets; Hyperforin: 10 targets. (B) Shortest-path
417 proximity (d_c) to 82 DILI-associated genes. Hyperforin is physically closer ($d_c = 1.30$) than Quercetin ($d_c = 1.68$).
418 Z-scores represent deviation from degree-matched null expectation ($n = 1,000$ permutations). Quercetin: $Z =$
419 -5.44 ($p < 0.001$); Hyperforin: $Z = -3.86$ ($p < 0.001$). Negative Z-scores indicate closer-than-random proximity.
420 Network: STRING v12.0 (confidence ≥ 900), GTEx v8 (liver TPM ≥ 1).

421 **Figure 2. Instability of proximity Z-scores.** Dumbbell plot showing the dissociation between shortest-path
422 proximity (left) and random walk influence (right) at STRING confidence ≥ 900 . At this threshold, Quercetin
423 appears more "significant" in Z-score but is physically more distant (1.68 vs 1.30) from DILI genes. Hyperforin:
424 proximity $Z = -3.86$, influence $Z = +10.12$ ($p < 0.001$). Quercetin: proximity $Z = -5.44$, influence $Z = +4.55$
425 ($p < 0.001$). Influence quantified by random walk with restart (RWR; $\alpha = 0.15$). $n = 1,000$ degree-matched
426 permutations per compound.

427 **Figure 3. Expression weighting refines influence propagation.** Waterfall decomposition of Z-score changes
428 under expression-weighted influence (EWI). Initial Hyperforin advantage: $\Delta Z = +5.57$ (RWR). Hyperforin change:
429 -1.14 (attenuation of signal through liver-active hubs). Quercetin change: $+1.24$ (gain from high-expression
430 nodes like CFB). Residual Hyperforin advantage: $\Delta Z = +3.19$. Both compounds remain significant under EWI:
431 Hyperforin $Z = +8.98$ ($p < 0.001$); Quercetin $Z = +5.79$ ($p < 0.001$). Expression weighting from GTEx v8 liver
432 tissue.

433 **Figure 4. Average network influence quantifies efficiency disparity.** Phase plot of total influence versus
434 target count. Horizontal lines represent efficiency tiers (Efficiency/average influence = constant). Hyperforin
435 occupies a higher efficiency region despite fewer targets. Efficiency/average influence values: Hyperforin = 0.1138
436 (RWR), 0.1330 (EWI); Quercetin = 0.0322 (RWR), 0.0493 (EWI). Efficiency difference: $3.7 \times$ (based on bootstrap
437 mean comparison). The observed influence represents an effect-size normalization (total steady-state mass on DILI
438 genes); no independent permutation test was performed.

439 **Figure 5. Bootstrap sensitivity analysis excludes target-count confounding.** Density distribution of RWR
440 influence scores from 100 random 10-target samples drawn from Quercetin's 62-target pool. Shaded region: 95%
441 confidence interval (0.0160–0.0542). Vertical line: Hyperforin observed influence (0.1138). Hyperforin exceeds
442 the entire bootstrap distribution ($3.7 \times$ fold vs. mean). This confirms that Hyperforin's advantage is not attributable
443 to favorable target count. Bootstrap is a robustness control; it does not provide independent statistical evidence.

444 **Figure 6. Chemical similarity control excludes structural confounding.** Maximum Tanimoto similarity to
445 DILrank reference drugs. Reference set: 542 DILI-positive, 365 DILI-negative drugs. Hyperforin: max = 0.15
446 (DILI+), 0.20 (DILI-). Quercetin: max = 0.21 (DILI+), 0.22 (DILI-). Dashed line: 0.4 threshold for structural
447 analog detection [19]. Neither compound is a structural analog of known hepatotoxins. This orthogonal analysis
448 excludes chemical class as an explanation for the observed network signal. Fingerprints: Morgan (ECFP4), radius
449 2, 2048 bits.

450 **Tables**

Table 1: Network metrics reveal the instability of proximity Z-scores. While Quercetin achieves more significant proximity Z-scores due to tighter null distributions, Hyperforin is physically closer (d_c) to DILI genes. Influence-based metrics resolve this confounding and stably prioritize Hyperforin. Network: STRING v12.0 LCC (confidence ≥ 900) filtered to liver-expressed genes.

| Metric | Compound | Targets | Observed | Z-score | P-value | Efficiency |
|---|------------|---------|--------------|---------------|----------|------------|
| <i>Tier 1: Shortest-path proximity</i> | | | | | | |
| | Hyperforin | 10 | $d_c = 1.30$ | -3.86 | < 0.001* | — |
| | Quercetin | 62 | $d_c = 1.68$ | -5.44 | < 0.001* | — |
| <i>Instability: Quercetin is physically more distant yet more "significant"</i> | | | | | | |
| <i>Tier 2: Random walk influence (RWR)</i> | | | | | | |
| | Hyperforin | 10 | 0.1138 | +10.12 | < 0.001* | 0.1138 |
| | Quercetin | 62 | 0.0322 | +4.55 | < 0.001 | 0.0322 |
| <i>Resolution: Correctly prioritizes physical proximity and regulatory hub modulation</i> | | | | | | |
| <i>Tier 3: Expression-weighted influence (EWI)</i> | | | | | | |
| | Hyperforin | 10 | 0.1330 | +8.98 | < 0.001* | 0.1330 |
| | Quercetin | 62 | 0.0493 | +5.79 | < 0.001 | 0.0493 |

*At permutation floor (<1/1,000).

Efficiency = average influence per target; RWR = random walk with restart; EWI = expression-weighted influence; d_c = mean minimum shortest-path distance; DILI = drug-induced liver injury. All associations survived Benjamini–Hochberg FDR correction ($q < 0.05$).

Table 2: Average influence efficiency. Normalization to the total seeding mass quantifies the average influence per target. Hyperforin targets are 3.7-fold more efficient at perturbing the DILI module than Quercetin targets.

| Analysis | Hyp. Eff. | Quer. Eff. | Eff. Ratio* | Rob. Ratio† |
|---------------------------|-----------|------------|-------------|-------------|
| RWR (topology-only) | 0.1138 | 0.0322 | 3.5× | 3.7× |
| EWI (expression-weighted) | 0.1330 | 0.0493 | 2.7× | 2.8× |

*Efficiency Ratio = Observed average influence ratio. †Robust Ratio = Observed influence / size-matched Bootstrap Mean (N=10). RWR = random walk with restart; EWI = expression-weighted influence.

Table 3: **Bootstrap sensitivity excludes target-count confounding.** Random 10-target subsets ($n = 100$) sampled without replacement from Quercetin’s 62-target pool. Hyperforin’s observed influence exceeds the entire bootstrap distribution.

| Statistic | Value | Interpretation |
|---------------------|------------------|--------------------------------|
| Hyperforin observed | 0.1138 | Reference |
| Bootstrap mean | 0.0308 | Expected if targets equivalent |
| Bootstrap SD | 0.0100 | Sampling variability |
| Bootstrap 95% CI | [0.0160, 0.0542] | 2.5th–97.5th percentile |
| Hyperforin / mean | 3.7× | Effect size |
| Exceeds 95% CI? | Yes | Not attributable to sampling |

Random seed: 42. Note: Bootstrap confirms robustness to target selection; it does not constitute independent inferential evidence.

Table 4: **Chemical similarity excludes structural confounding.** Neither compound resembles known hepatotoxins ($\text{Tanimoto} < 0.4$). Quercetin is more similar to DILI-positive drugs yet shows lower network influence.

| Compound | Max Tanimoto (DILI+) | Max Tanimoto (DILI-) | Analog?* | Network rank |
|------------|----------------------|----------------------|----------|----------------------|
| Hyperforin | 0.154 | 0.202 | No | 1 (higher influence) |
| Quercetin | 0.212 | 0.220 | No | 2 (lower influence) |

*Analog threshold: $\text{Tanimoto} > 0.4$ (Maggiora et al., 2014). Morgan fingerprints (ECFP4, radius 2, 2048 bits). DILIRank: 542 DILI+, 365 DILI- drugs.

Table 5: **Hyperforin targets include regulatory hubs.** All 10 Hyperforin targets in the liver-expressed LCC, with liver expression (GTEx v8) and network degree. PXR (NR1I2) is the master regulator; CYP enzymes are downstream effectors.

| Gene | Protein | TPM | Degree | Function | DILI link |
|--------|---------|-----|------------|-----------------------|-----------|
| NR1I2 | PXR | 43 | 28 | Master regulator | Direct |
| CYP3A4 | CYP3A4 | 335 | 89 | Xenobiotic metabolism | Direct |
| CYP2C9 | CYP2C9 | 434 | 76 | Xenobiotic metabolism | Direct |
| CYP2B6 | CYP2B6 | 125 | 42 | Xenobiotic metabolism | Indirect |
| AKT1 | PKB | 33 | 312 | Stress signaling | Indirect |
| ABCB1 | P-gp | 7 | 53 | Drug efflux | Direct |
| ABCC2 | MRP2 | 60 | 38 | Drug efflux | Direct |
| ABCG2 | BCRP | 4 | 31 | Drug efflux | Indirect |
| MMP2 | MMP2 | 5 | 87 | ECM remodeling | Indirect |
| MMP9 | MMP9 | 1 | 94 | ECM remodeling | Indirect |

AKT1 is the highest-degree target (312 neighbors). Five of 10 targets (NR1I2, CYP3A4, CYP2C9, ABCB1, ABCC2) are directly connected to DILI genes. TPM = transcripts per million; DILI = drug-induced liver injury; LCC = largest connected component.

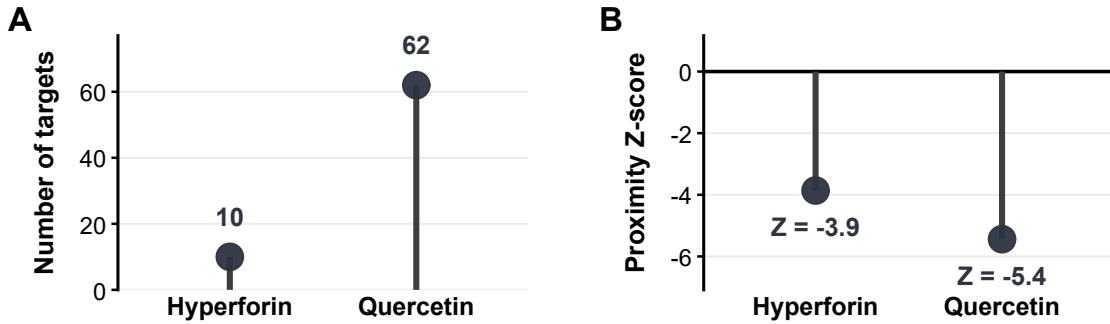
Table 6: **Influence ranking is robust to network construction parameters.** Hyperforin ranks first across all thresholds and influence metrics. Proximity Z-scores are unstable and reverse rankings between thresholds, failing to accurately reflect the physical distance advantage of Hyperforin.

| Threshold | Compound | RWR Z | EWI Z | Proximity d_c | Proximity Z |
|------------------------------|------------|---------------|--------|-----------------|-------------|
| ≥ 700 (11,693 nodes) | Hyperforin | +12.08 | +11.20 | 0.60 | -6.04 |
| | Quercetin | +5.53 | +7.09 | 1.34 | -5.46 |
| ≥ 900 (7,677 nodes) | Hyperforin | +10.12 | +8.98 | 1.30 | -3.86 |
| | Quercetin | +4.55 | +5.79 | 1.68 | -5.44 |

Note: At ≥ 900 , Quercetin achieves a more "significant" proximity Z-score despite being physically more distant (1.68 vs 1.30) from DILI genes. RWR = random walk with restart; EWI = expression-weighted influence; d_c = mean minimum shortest-path distance; DILI = drug-induced liver injury.

451 **Figures**

Network context: target count and proximity to DILI genes

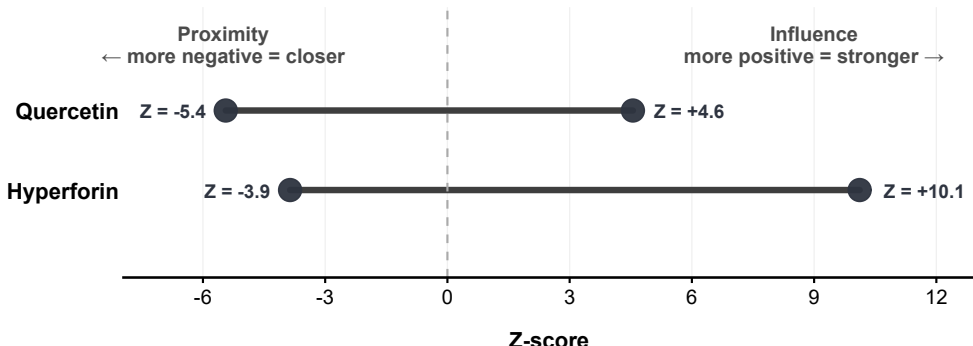


[DESCRIPTIVE CONTEXT] Target count and shortest-path proximity provide network context but are not used for causal inference. Proximity Z-scores represent deviation from degree-matched random expectation ($n = 1,000$ permutations). Negative values indicate closer-than-random proximity. Data: STRING v12.0 (≥ 900), human liver LCC.

Figure 1: Network context: target count and physical proximity to DILI genes. (A) Target count in the liver-expressed largest connected component. Quercetin: 62 targets; Hyperforin: 10 targets. (B) Shortest-path proximity (d_c) to 82 DILI-associated genes. Hyperforin is physically closer ($d_c = 1.30$) than Quercetin ($d_c = 1.68$). Z-scores represent deviation from degree-matched null expectation ($n = 1,000$ permutations). Quercetin: $Z = -5.44$ ($p < 0.001$); Hyperforin: $Z = -3.86$ ($p < 0.001$). Negative Z-scores indicate closer-than-random proximity. Network: STRING v12.0 (confidence ≥ 900), GTEx v8 (liver TPM ≥ 1).

Proximity does not predict influence

Proximity ranking is threshold-dependent; influence ranking is stable

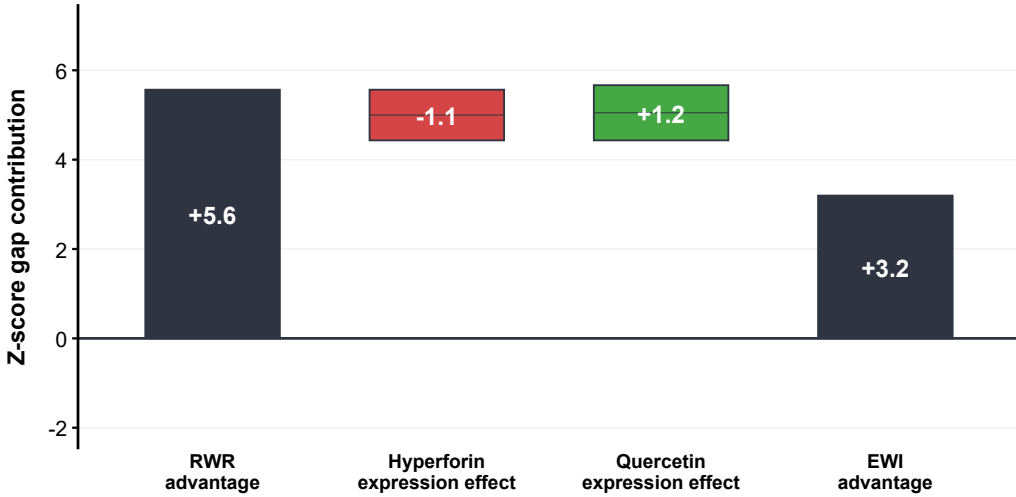


[CORE INFERENCE] The rank reversal demonstrates that shortest-path proximity does not predict functional influence. Lines connect each compound's proximity Z-score with its influence Z-score (random walk with restart, RWI). Both metrics derived from degree-matched permutation null models ($n = 1,000$). Data: STRING v12.0 (≥ 900).

Figure 2: **Instability of proximity Z-scores.** Dumbbell plot showing the dissociation between shortest-path proximity (left) and random walk influence (right) at STRING confidence ≥ 900 . At this threshold, Quercetin appears more "significant" in Z-score but is physically more distant (1.68 vs 1.30) from DILI genes. Hyperforin: proximity $Z = -3.86$, influence $Z = +10.12$ ($p < 0.001$). Quercetin: proximity $Z = -5.44$, influence $Z = +4.55$ ($p < 0.001$). Influence quantified by random walk with restart (RWR; $\alpha = 0.15$). $n = 1,000$ degree-matched permutations per compound.

Expression weighting attenuates but does not reverse the advantage

Gap: +5.6 (RWR) → +3.2 (EWI)

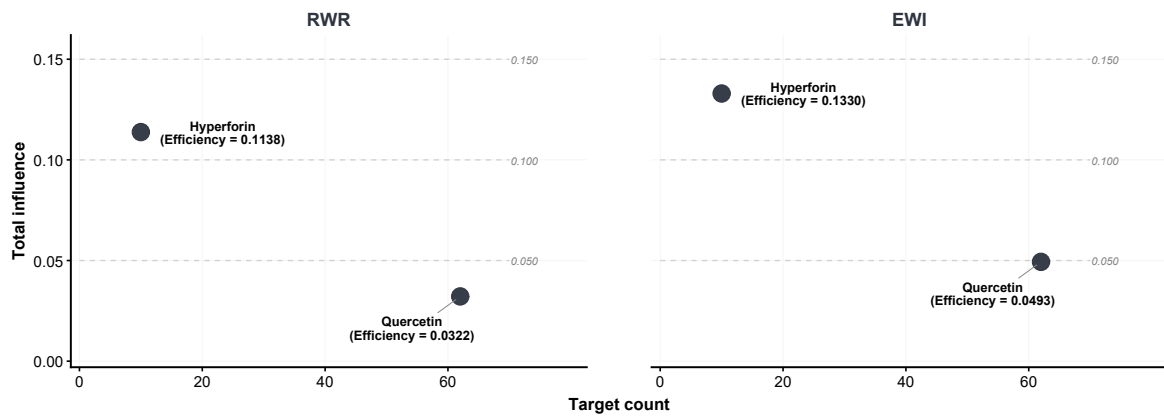


[CONSTRAINT ANALYSIS] The RWR advantage (+5.6) is partitioned under expression-weighted influence propagation:
 (1) Hyperforin's change under expression weighting (-1.1); (2) Quercetin's gain (+1.2, driven by CFB at 1115
 TPM). Residual advantage (+3.2) remains significant (both $p < 10^{-8}$). GTEx v8 liver expression (TPM ≥ 1). STRING
 v12.0 (≥ 900), $n = 1,000$ degree-matched permutations.

Figure 3: Expression weighting refines influence propagation. Waterfall decomposition of Z-score changes under expression-weighted influence (EWI). Initial Hyperforin advantage: $\Delta Z = +5.57$ (RWR). Hyperforin change: -1.14 (attenuation of signal through liver-active hubs). Quercetin change: $+1.24$ (gain from high-expression nodes like CFB). Residual Hyperforin advantage: $\Delta Z = +3.19$. Both compounds remain significant under EWI: Hyperforin $Z = +8.98$ ($p < 0.001$); Quercetin $Z = +5.79$ ($p < 0.001$). Expression weighting from GTEx v8 liver tissue.

Average network influence quantifies perturbation efficiency

Normalization reframes polypharmacology as efficiency, not coverage

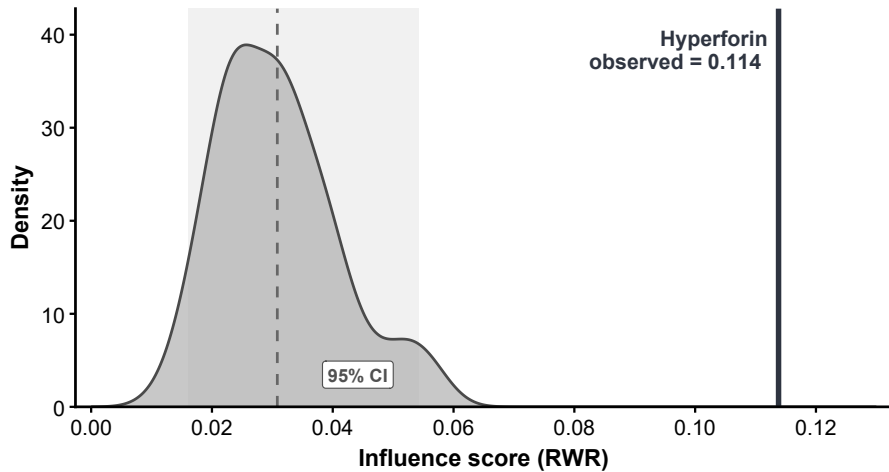


Average influence represents an effect-size normalization (total steady-state mass on DILI genes); no independent permutation test was performed. Horizontal lines represent efficiency tiers (Average Influence = constant). Hyperforin occupies a higher efficiency region despite fewer targets. Data: STRING v12.0 (≥ 900), $n = 1,000$ permutations.

Figure 4: Average network influence quantifies efficiency disparity. Phase plot of total influence versus target count. Horizontal lines represent efficiency tiers (Efficiency/average influence = constant). Hyperforin occupies a higher efficiency region despite fewer targets. Efficiency/average influence values: Hyperforin = 0.1138 (RWR), 0.1330 (EWI); Quercetin = 0.0322 (RWR), 0.0493 (EWI). Efficiency difference: **3.7 \times** (based on bootstrap mean comparison). The observed influence represents an effect-size normalization (total steady-state mass on DILI genes); no independent permutation test was performed.

Bootstrap sensitivity analysis excludes target-count confounding

Distribution of influence scores from random 10-target samples



[ROBUSTNESS CONTROL] Bootstrap sensitivity: 100 random 10-target samples from Quercetin's pool, scored by random walk with restart (RWI). Shaded = 95% CI. Hyperforin (solid line) exceeds entire distribution. Data: STRING v12.0 (≥ 900).

Figure 5: **Bootstrap sensitivity analysis excludes target-count confounding.** Density distribution of RWR influence scores from 100 random 10-target samples drawn from Quercetin's 62-target pool. Shaded region: 95% confidence interval (0.0160–0.0542). Vertical line: Hyperforin observed influence (0.1138). Hyperforin exceeds the entire bootstrap distribution ($3.7 \times$ fold vs. mean). This confirms that Hyperforin's advantage is not attributable to favorable target count. Bootstrap is a robustness control; it does not provide independent statistical evidence.

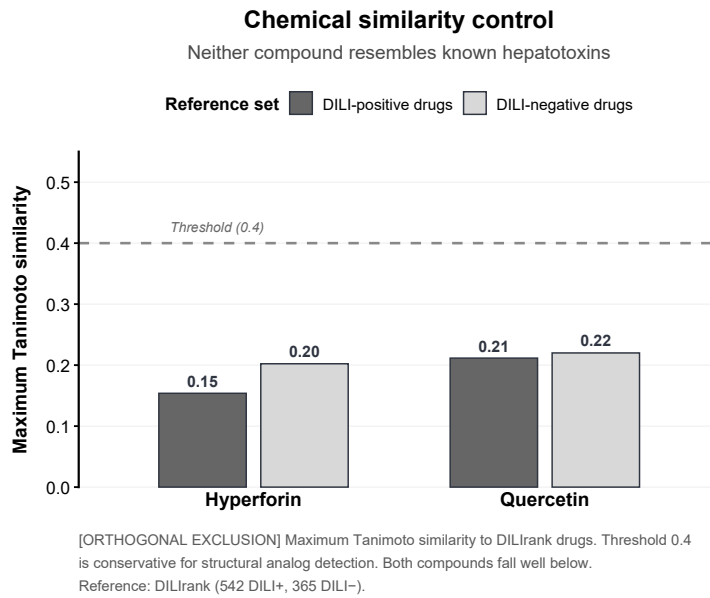


Figure 6: Chemical similarity control excludes structural confounding. Maximum Tanimoto similarity to DILIRank reference drugs. Reference set: 542 DILI-positive, 365 DILI-negative drugs. Hyperforin: max = 0.15 (DILI+), 0.20 (DILI-). Quercetin: max = 0.21 (DILI+), 0.22 (DILI-). Dashed line: 0.4 threshold for structural analog detection [19]. Neither compound is a structural analog of known hepatotoxins. This orthogonal analysis excludes chemical class as an explanation for the observed network signal. Fingerprints: Morgan (ECFP4), radius 2, 2048 bits.

452 **Author contributions**

453 **Antony Bevan:** Conceptualization, Methodology, Software, Validation, Formal analysis, Investigation, Data Cu-
454 ration, Writing - Original Draft, Writing - Review & Editing, Visualization.

455 **Acknowledgements**

456 This research received no external funding. AI-assisted tools were used to assist with code development and
457 statistical analysis. The author takes full responsibility for all content.

458 **Competing interests**

459 The author(s) declare no competing interests.

460 **Supplementary Tables**

Table S1: **Hyperforin target genes and literature sources.** All 14 raw targets with UniProt IDs, gene symbols, and primary literature sources. Targets marked with * are present in the liver-expressed LCC (STRING ≥ 900 , GTEx TPM ≥ 1).

| UniProt | Gene | In LCC | Source |
|----------------|-------------|---------------|---------------|
| O75469 | NR1I2 (PXR) | Yes* | [6, 9] |
| P08684 | CYP3A4 | Yes* | [6] |
| P11712 | CYP2C9 | Yes* | [20] |
| P20813 | CYP2B6 | Yes* | [21] |
| P08183 | ABCB1 | Yes* | [22] |
| Q9UNQ0 | ABCG2 | Yes* | [23] |
| O15440 | ABCC2 | Yes* | [24] |
| P31749 | AKT1 | Yes* | [25] |
| P08253 | MMP2 | Yes* | [25] |
| P14780 | MMP9 | Yes* | [26] |
| Q9Y210 | TRPC6 | No | [27] |
| P15692 | VEGFA | No | [26] |
| Q13794 | PMAIP1 | No | [28] |
| Q12879 | GRIN1 | No | [29] |

Table S2: **Quercetin target curation summary.** Target counts at each processing stage.

| Stage | Count |
|--|--------------|
| Raw targets (ChEMBL v31, CHEMBL159) | 122 |
| Excluded: non-human (mouse, rat, bacterial, viral) | 10 |
| Excluded: no UniProt mapping | 25 |
| Processed targets | 87 |
| Excluded: not liver-expressed (TPM < 1) | 20 |
| Excluded: not in STRING LCC | 5 |
| Final targets in LCC | 62 |

Table S3: **DILI gene set curation.** Genes associated with drug-induced liver injury from DisGeNET (UMLS C0860207).

| Stage | Count |
|---------------------------------------|-------|
| Raw DILI genes (DisGeNET) | 127 |
| In STRING ≥ 700 liver LCC | 84 |
| In STRING ≥ 900 liver LCC | 82 |
| Excluded: miRNAs (not in PPI network) | 21 |
| Excluded: cytokines (not in LCC) | 12 |
| Excluded: other | 12 |

Table S4: **Genes targeted by both compounds.** Five genes present in both Hyperforin and Quercetin target sets.

| Gene | Protein | Function |
|--------|----------------------------|---------------------------------|
| ABCG2 | BCRP | Efflux transporter |
| AKT1 | Protein kinase B | Cell survival signaling |
| CYP3A4 | Cytochrome P450 3A4 | Drug metabolism |
| MMP2 | Matrix metalloproteinase-2 | Extracellular matrix remodeling |
| MMP9 | Matrix metalloproteinase-9 | Extracellular matrix remodeling |

Table S5: **Direct DILI gene connectivity.** Hyperforin targets with first-order (distance = 1) connections to DILI genes in the STRING network (≥ 900). DILI neighbors are genes present in the 82-gene DILI set.

| Target | DILI Neighbors | N | Function |
|---------------------|-------------------------------------|-----------|-----------------------|
| CYP3A4 | NR1I2, CYP2E1, UGT1A9, GSTM1, GSTP1 | 5 | Xenobiotic metabolism |
| AKT1 | MAP3K5, NFE2L2, CTNNB1, IGF1 | 4 | Stress response |
| MMP9 | LCN2, SPP1, MMP2 | 3 | Inflammation/ECM |
| ABCB1 | ABCC2, NR1I2 | 2 | Drug transport |
| CYP2C9 | CYP2E1, NR1I2 | 2 | Xenobiotic metabolism |
| CYP2B6 | NR1I2 | 1 | Xenobiotic metabolism |
| NR1I2 | CYP2E1, ABCC2 | 2 | Master regulator |
| ABCG2 | ABCC2 | 1 | Drug transport |
| ABCC2 | NR1I2, ABCB1 | 2 | Drug transport |
| MMP2 | MMP9, SPP1 | 2 | ECM remodeling |
| Total unique | | 12 | |

Table S6: **Quercetin direct DILI gene connectivity summary.** Summary statistics for first-order DILI connections across Quercetin's 62 targets.

| Metric | Value |
|--|--------------|
| Total targets in LCC | 62 |
| Targets with ≥ 1 direct DILI neighbor | 18 |
| Total direct DILI connections | 31 |
| Mean DILI neighbors per target | 0.50 |
| <i>Hyperforin comparison:</i> | |
| Hyperforin targets with ≥ 1 DILI neighbor | 10/10 (100%) |
| Mean DILI neighbors per Hyperforin target | 2.4 |

Table S7: **Quercetin target genes in the liver-expressed network.** All 62 Quercetin targets in STRING v12.0 LCC (confidence ≥ 900) with liver TPM ≥ 1 (GTEX v8). Sorted by descending liver expression.

| Gene | TPM | Gene | TPM | Gene | TPM | Gene | TPM |
|--------|------|----------|-----|----------|-----|--------|-----|
| CFB | 1115 | CYP3A4 | 335 | FN1 | 229 | ALDH2 | 183 |
| ANPEP | 160 | PPIA | 112 | SERPINA5 | 104 | CYP1A2 | 72 |
| CA2 | 64 | APP | 63 | PYGL | 55 | HDAC6 | 45 |
| ESRRRA | 42 | MAOA | 35 | AKR1C2 | 33 | AKT1 | 33 |
| CTSH | 28 | XDH | 26 | CHRNA4 | 25 | PIK3R1 | 24 |
| PIM1 | 24 | LDLR | 23 | EGFR | 17 | ELOVL1 | 18 |
| PKN1 | 16 | GSK3A | 13 | YES1 | 13 | MET | 12 |
| DAPK1 | 12 | BACE1 | 11 | CSNK2A1 | 10 | FSTL1 | 9 |
| SIRT6 | 8 | GSK3B | 7 | CDK7 | 7 | CAV2 | 7 |
| PTPN2 | 6 | CYP1A1 | 5 | PRMT7 | 5 | MMP2 | 5 |
| AKR1B1 | 5 | PDE6D | 5 | PTK2 | 4 | ABCG2 | 4 |
| IQGAP1 | 4 | ADRB2 | 3 | BRAF | 4 | KDR | 3 |
| SRC | 3 | ALOX5 | 3 | CYP1B1 | 3 | TLR4 | 3 |
| NUAK1 | 3 | AXL | 2 | ADA | 2 | LCK | 2 |
| ABCC1 | 2 | PLK1 | 1 | ACHE | 1 | MMP9 | 1 |
| SYK | 1 | PDZK1IP1 | 1 | | | | |

Table S8: **DILI gene set (82 genes).** Genes in STRING v12.0 LCC (confidence ≥ 900) with liver TPM ≥ 1 (GTEX v8). Source: DisGeNET (UMLS C0860207). Sorted alphabetically.

| 82 DILI-Associated Genes | | | | | | | |
|--------------------------|----------|--------|--------|--------|--------|---------|--------|
| ABCB1 | AHR | ALB | ALDOB | AMBP | APOA1 | APOE | APOH |
| ARG1 | ARNT | ATG5 | BAX | BTD | C3 | CAT | CCL2 |
| CLU | COL3A1 | CTNNB1 | CXCL1 | CXCL10 | CYP2A6 | CYP2C19 | CYP2C9 |
| CYP2E1 | DGAT2 | ENO1 | FGA | FLT1 | FMO3 | GADD45A | GC |
| GCLC | GPT | GSN | GSTM1 | GSTM2 | GSTP1 | HLA-A | HLA-B |
| HLA-DQB1 | HLA-DRB1 | HMGBl | HMOX1 | HPD | HPX | IGF1 | IL18 |
| IL1R2 | KRT18 | LCN2 | LGALS3 | MAP3K5 | MED1 | MMP2 | MTHFR |
| NAT2 | NFE2L2 | NR1H3 | NR1H4 | NR1I2 | NR1I3 | PLAT | PLG |
| PNP | POLG | PON1 | PPARA | PRKDC | PTGS2 | RBP1 | SLPI |
| SNX18 | SOD1 | SOD3 | SPP1 | TALDO1 | TBXA2R | TCTN1 | TF |
| TTR | UGT1A9 | | | | | | |

Table S9: **Null distribution parameters from permutation testing.** Null distribution parameters (mean and standard deviation) from $n = 1,000$ degree-matched permutations. Note the tightening of the Quercetin null distribution as the number of targets increases, which drives the inflation of proximity Z-scores.

| Metric | Compound | μ_{null} | σ_{null} | x_{obs} | Z-score |
|---|-----------------|--------------|-----------------|-----------|---------|
| <i>Shortest-path proximity (at ≥ 900)</i> | | | | | |
| | Hyperforin (10) | 2.21 | 0.235 | 1.30 | -3.86 |
| | Quercetin (62) | 2.17 | 0.091 | 1.68 | -5.44 |
| <i>Random walk influence (at ≥ 900)</i> | | | | | |
| | Hyperforin (10) | 0.0147 | 0.0098 | 0.1138 | +10.12 |
| | Quercetin (62) | 0.0148 | 0.0038 | 0.0322 | +4.55 |
| <i>Expression-weighted influence (at ≥ 900)</i> | | | | | |
| | Hyperforin (10) | 0.0205 | 0.0125 | 0.1330 | +8.98* |
| | Quercetin (62) | 0.0209 | 0.0049 | 0.0493 | +5.79* |

*Significance remains high despite tissue-specific attenuation. μ_{null} = null distribution mean; σ_{null} = null distribution standard deviation; x_{obs} = observed metric value.